CW threshold characteristics of Coupled-Cavity VCSELs: experiment and model

Mateusz Zujewski, Leszek Frasunkiewicz, Kent Choquette, Tomasz Czyszanowski, Hugo Thienpont, Krassimir Panajotov

***Abstract*—We carry out a detailed characterization of CW threshold behaviour of Coupled-Cavity VCSELs with various radii of the ion-implantation and oxide apertures. We obtain modal threshold current maps and wavelength at threshold and identify four groups of lasers with qualitatively different behavior, i. e. lasing only on the short, on the long or on both short and long wavelength fundamental modes. All lasers show profound impact of the current induced self-heating. In order to elucidate this impact, we improve the existing rate equation model by considering nonuniform longitudinal temperature distribution and adding the gain and refractive index temperature dependencies. We are able to reproduce the experimentally observed switchings between different longitudinal modes, as well as all the four different types of modal behavior.**

***Index Terms*—VCSEL, Coupled Cavities, Rate Equations**

I. Introduction

Vertical-Cavity Surface-Emitting Lasers (VCSEL) are prominent light-source candidates for cost-effective optical systems due to their advantageous properties, such as 2D array mass production, on wafer testing, low power consumption, single longitudinal mode operation and circular beam emission [1]–[4]. Among them, Coupled-Cavity (CC) VCSELs (also called Compound-Resonator VCSELS) consisting of two optical cavities separated by a middle Distributed Bragg Reflector (DBR), have attracted considerable attention recently. CC-VCSELs were first realized by Stanley et al. in 1994 [5] and shown to support two longitudinal resonant modes. The splitting between these modes depends on the cavity detuning and on the cavity coupling strength, i. e. on the transmission of the middle DBR [5], [6]. As the two cavities can be independently biased, lasing may occur on either the long or the short wavelength mode, or on the two modes simultaneously [7]–[12]. This allows using one of the cavities as an active lasing source and the second one as an electro-absorption (EA) or electro-refraction (ER) modulator. This new degree of freedom has been utilized to achieve fast voltage-controlled polarization or wavelength switching [13]–[15]. Tailoring the emission wavelength of the CC-VCSEL with respect to the absorber band-edge provides new possibilities, such as efficient intensity modulation, optical bistable operation and self-pulsations [16]–[18]. Bistable output has been observed in continuous wave (CW) operation and explained by the absorption resonance shift due to the joule heating of the laser [19]. Using a bulk material in one of the cavities an enhanced absorption, Q-switching and intensity modulation have been demonstrated [9], [20].

The CC-VCSELs' characteristics investigated in [21] show threshold current changes in one cavity due to current injection in the other one. Also a strong longitudinal mode competition has been reported [22]. The threshold curves for the two longitudinal modes in the plane of the two injection currents, as well as the double threshold point have been identified in [11], [13], [23] for the case of slightly detuned CC-VCSELs. The experimental characteristics in pulse regime show very good agreement with theory [11] without the need of taking into account the current induced self-heating. In CW regime however, the temperature rise due to this self-heating impacts strongly the longitudinal mode threshold charactersitics as shown in [24]. The goal of this paper is to investigate in details this impact and present a way to model it. To this aim, we extend the CC-VCSEL model of [11] by considering in a simple way the nonuniform temperature distribution along the CC-VCSEL structure and its impact on the gain and refractive indices. Our improved model allows simulation of the CC-VCSEL threshold behavior in a CW mode in good agreement with experiment as shown hereafter.

II. Experiment

We characterize a wafer consisting of several units of CC-VCSELs. There are 100 different lasers in each unit with varying apertures of the top ion implantation and bottom oxidation. The lasers have been subject to light-current and spectral characterization with the setup schematically presented in Fig. 1. The two channels CH1 and CH2 are used to independently connect the top and the bottom cavity with the laser driver (LD). The threshold modal behavior is analyzed with the power meter (PM) and optical spectrum analyzer (OSA).

A. Longitudinal mode threshold map

To illustrate the CC-VCSELs behavior we map the threshold for single transverse mode operation and the onset of multi-transverse mode operation in the plane of the two injection

Manuscript received 2013; revised 2013. This work was supported by FWO-Vlaanderen project G.0657.09N and OZR-VUB.

M. Zujewski, L. Frasunkiewicz, H. Thienpont and K. Panajotov are with Vrije Universiteit Brussel, Faculty of Engineering Sciences, Brussels Photonics Team B-PHOT, Pleinlaan 2, 1050 Brussels, Belgium, (mzujewsk@b-phot.org, lfrasunk@b-phot.org, hthienpo@b-phot.org, kpanajot@b-phot.org).

K. Panajotov is also with Institute of Solid State Physics, 72 Tzarigradsko Chaussee Blvd., 1784 Sofia, Bulgaria.

K. Choquette is with the University of Illinois at Urbana-Champaign, Urbana, IL 61801 USA.

T. Czyszanowski and L. Frasunkiewicz are with the Institute of Physics, Technical University of Lodz, ul. Wolczanska 219, 93-005 Lodz, Poland.

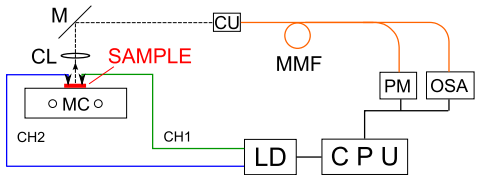

Fig. 1. Experimental Setup. CL is a collimating lens, M - mirror, CU - coupling unit, MMF - multimode fibre, PM - power meter, OSA - optical spectrum analyzer, LD - laser driver and MC - micromanipulators.

currents in the bottom and top cavity. We find out that the obtained results can be collected in 4 groups depending mainly on the oxidation aperture size, which varies from 2 x 2 μm^2 to 9 x 9μm^2. Fig. 2 shows a graphical representation of part of the wafer unit with the areas where each group can be found denoted (black letters). The white letters denote the locations of the representative lasers, which threshold characteristics are presented in the following subsections. This behavior pattern repeats in all wafer units.

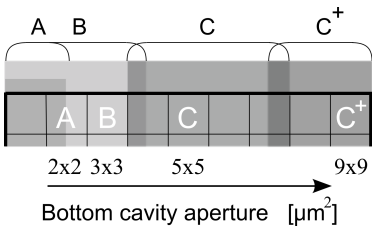

Fig. 2. Graphical representation of the 4 typical groups of CC-VCSELs in one unit on the wafer (top black letters A, B, C and C$^+$). The threshold characteristics of the lasers marked with the white letters are presented in the following subsections. The bottom aperture sizes are indicated below the picture.

1) Group A lasers: The CC-VCSELs from group A show only long wavelength fundamental mode emission in the measured range of currents. In Fig. 3 the threshold current map of laser A with 5 x 5 μm^2 top and 2 x 2 μm^2 bottom current aperture is presented. As can be seen, the threshold current curve for the fundamental mode (denoted by open triangles) shows a typical parabolic shape. Remarkably, the onset of multi transverse-mode emission (denoted by half open triangles) is almost independent on I_{BOT} and takes place at $I_{TOP} \approx 2.7$ mA. The region of fundamental mode operation is situated between these two curves and is denoted by $\lambda_{Lsingle}$. Also shown on this map is the dependence of wavelength of emission at the threshold points denoted by $1, 2, 3...n$ and corresponding to threshold current points denoted by $1', 2', 3'...n'$.

2) Group B lasers: The CC-VCSELs from group B show dual wavelength mode emission in the measured range of currents. In Fig. 4 the threshold map of laser B with 6 x 6 μ^2m top and 3 x 3 μm^2 bottom current aperture is shown. On the map, we see regions of single longitudinal mode emission on either the short (denoted by λ_S) or the long (denoted by λ_L) wavelength fundamental mode. There are two regions of dual mode emission (denoted by λ_{S+L}) . The onset of multimode emission is not independent on I_{BOT} as in the previous A group lasers. The modal behavior of group B lasers

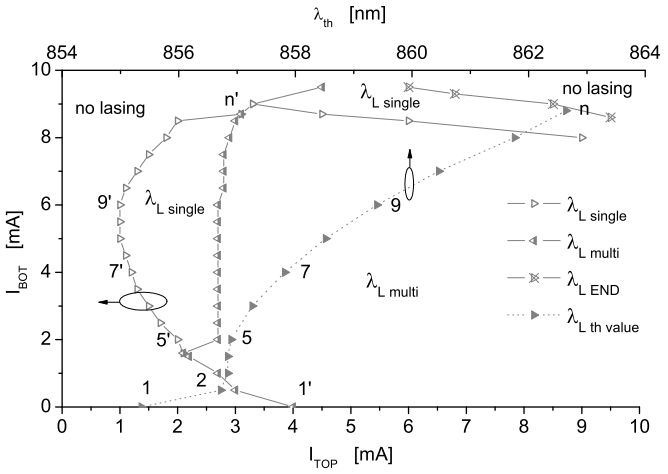

Fig. 3. Long wavelength threshold characteristics of group A laser. The threshold current curves for the fundamental and first order modes are denoted by open and half open triangles. The region of fundamental mode operation is situated between these two curves and is denoted by $\lambda_{Lsingle}$. The emission wavelength points marked by $1, 2, 3...n$ correspond to threshold current points marked by $1', 2', 3'...n'$.

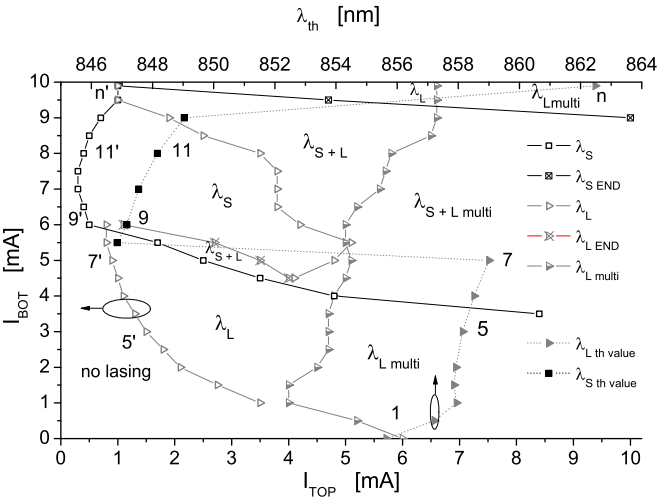

Fig. 4. Dual wavelength threshold characteristics of group B laser. Emission wavelengths and corresponding threshold current points marked as in Fig. 3.

is quite complex. For example, keeping the top cavity bias I_{TOP} = 3 mA and increasing the bottom cavity current, we observe multiple transitions between different transverse mode behavior. The laser reaches threshold for the long wavelength fundamental mode at $I_{BOT} \approx 1.6$ mA, then between 4.9 $< I_{BOT} <$ 5.5 mA we observe dual wavelength mode emission, between 5.5 $< I_{BOT} <$ 8.3 mA short wavelength fundamental-mode operation and for $I_{BOT} > 8.3$ mA again a dual wavelength mode operation.

3) Case C lasers: The CC-VCSELs from group C show a dual wavelength mode emission in the measured range of currents, however the long wavelength mode shifts strongly towards higher top-cavity injection currents. In Fig. 5 the map of laser C with 6 x 6 μm^2 top and 5 x 5 μ^2m bottom current aperture is shown. Here, we do not find the single long-wavelength fundamental-mode emission regime, instead for $I_{TOP} > 8$ mA we see lasing of the higher order long

wavelength mode. The threshold of the short wavelength mode for $I_{BOT} > 4$ mA is almost independent on the I_{TOP} injection current ($I_{TOP} \approx 0.4$ mA).

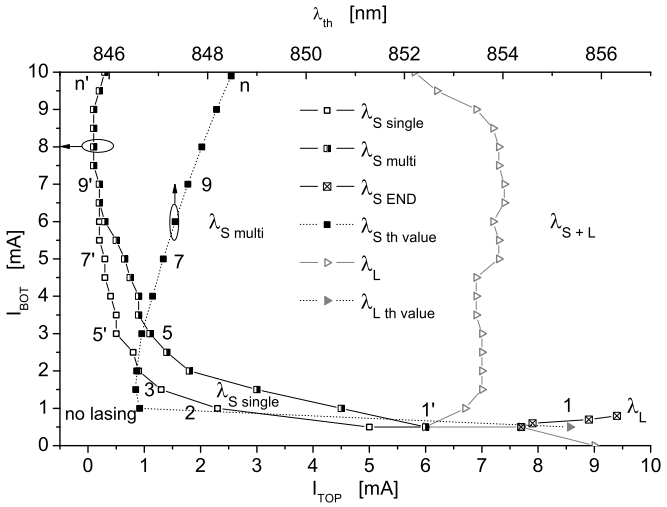

Fig. 5. Dual wavelength threshold characteristics of group C laser. Emission wavelengths and corresponding threshold current points marked as in Fig. 3.

4) Case C$^+$ lasers: The CC-VCSELs from group C$^+$ show only short-wavelength fundamental-mode emission in the measured range of currents. The long-wavelength fundamental-mode disappears, and the threshold current for the short-wavelength mode shifts towards higher injection currents on both cavities. In Fig. 6 the map of laser C$^+$ with 6 x 6 μm^2 top and 9 x 9 μ^2m bottom current aperture is shown.

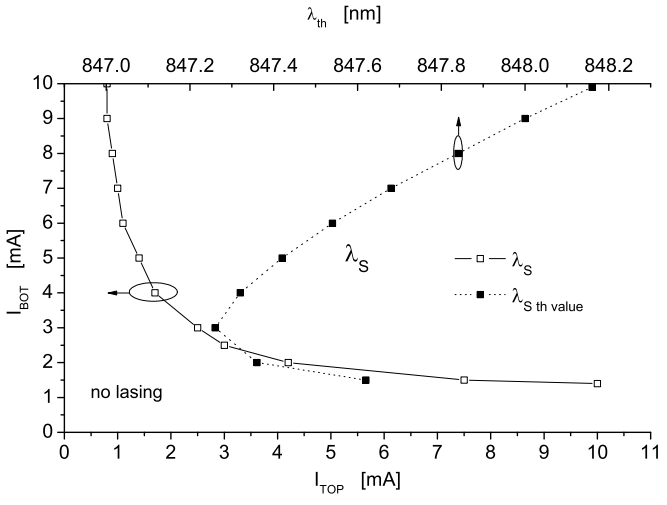

Fig. 6. Short wavelength threshold characteristics of group Cp laser. Emission wavelengths and corresponding threshold current points marked as in Fig. 3.

Group A lasers is a subgroup of group B structures. The same CC-VCSELs with identical top and bottom current apertures but from different units show either emission on only long-wavelength fundamental mode or on both short and long wavelength fundamental modes. In these two groups, we are able to identify double threshold points, areas of strong modal competition leading to switching between the two fundamental modes in a small range of currents, or disappearance of one mode in a double mode lasing regions. Lasers of this type seem to be very sensitive to small variations of their structures depending on the wafer position and therefore, it is hard to determine which of their parameters influence the threshold characteristics mostly. However, in theoretical modeling similar simplified mode lasing maps can be achieved. The behavior of lasers of types C and C+ is very similar for all the lasers in these groups and no significant effect of top implantation aperture size is observed.

III. CC-VCSEL Rate Equations

Following [11] we briefly summarize the derivation of the rate equations for the Coupled Cavity VCSEL. We use the reservoir model [4] to describe both carrier numbers N_1 and N_2 for the top ($i = 1$) and the bottom ($i = 2$) cavity and both photon numbers $N^S_{ph,1,2}$ and $N^L_{ph,1,2}$ of the short ($\lambda = S$) and the long ($\lambda = L$) wavelength mode.

The number of carriers reaching the QWs of the i^{th} cavity with injection efficiency η_i can be described as $\eta_i I_i/q$, where I_i is the current and q is the electric charge [4], [11]. After reaching the reservoir the carriers split into four groups that: 1) recombine in a nonradiative way, 2) recombine spontaneously, 3) experience stimulated emission and 4) experience stimulated absorption.

The photons in the photon reservoirs can be divided into three groups: 1) those that experience stimulated and spontaneous emission, 2) those that are absorbed in the active region and 3) those that are absorbed in the DBRs together with those that leave the cavity through the mirrors. Furthermore, the rate at which the photon population in each mode and cavity decays, can be expressed as: $N^{S,L}_{ph,1,2}/\tau_p h^{S,L}$, where the $\tau^{S,L}_{ph}$ describes the corresponding photon lifetimes [4], [11].

The stimulated emission ($R_{em,i}$) and the stimulated absorption ($R_{abs,i}$) induce changes of the carrier densities in the i^{th} cavity [4]: $R_{em,i} - R_{abs,i} = \Gamma^{\lambda}_{QW,i}\ v^{\lambda}_g\ N^{\lambda}_{ph}\ g^{\lambda}_i$. Here $\Gamma^{\lambda}_{QW,i}$ is the modal QW confinement factor calculated with 1D transfer matrix method [15], v^{λ}_g is the group velocity and g^{λ}_i describes the logarithmic gain [4].

The spontaneous ($R_{sp,i}$) and the nonradiative emission ($R_{nr,i}$) rates are proportional to the carrier densities in each cavity [11]: $R_{sp,i} - R_{nr,i} = n_i/\tau_e$. Here τ_e describes the carrier lifetime and the carrier density in cavity i is equal to $n_i = N_i/V_i$ with V_i being the volume of the active region in the i^{th} cavity.

Neglecting the photons coming from spontaneous emission to the lasing modes and in a steady state condition the rate equations for the carrier numbers are expressed as [11]:

$$\frac{\eta_i I_i}{q} = \left(\Gamma^{\lambda}_{QW,i}\ v^{\lambda}_g\ N^{\lambda}_{ph}\ g^{\lambda}_i\right) V_i + \frac{n_i V_i}{\tau_e} \tag{1}$$

and for the photon numbers as:

$$N^{\lambda}_{ph}\left(\Gamma^{\lambda}_{QW,i}\ v^{\lambda}_g\ g^{\lambda}_i - \frac{1}{\tau^{\lambda}_{ph}}\right) = 0. \tag{2}$$

Here: $i = 1, 2$ - denotes the top and bottom cavity, respectively and $\lambda = S, L$ - the short and the long wavelength mode.

The logarithmic gain as a function of carrier density n_i, temperature T and wavelength λ is expressed as [4], [11], [25]:

$$g_i^{\lambda}(n_i, T_i, \lambda_p) = G_{0,i} \ln \frac{n_i + n_0}{n_{tr,i} + n_0} - H_0(\lambda - \lambda_{p,i})^2 \quad (3)$$

with:

$$G_{0,i} = a_0 + a_1 T_i + a_2 T_i^2, \quad (4)$$

$$n_{tr,i} = b_0 + b_1 T_i, \quad (5)$$

and the gain peak wavelength $\lambda_{p,i}$ temperature dependence as:

$$\lambda_{p,i} = \lambda_0 + \lambda_1 T_i. \quad (6)$$

Here $n_{tr,i}$ is the carrier transparency density and n_0 - a gain fitting parameter describing the absorption in the QWs α^{λ} [4]

$$\alpha^{\lambda} = G_{0,i} \ln \frac{n_0}{n_{tr,i} + n_0} - H_0(\lambda - \lambda_{p,i})^2. \quad (7)$$

The coefficients $H_0, a_0, a_1, a_2, b_0, b_1, \lambda_0$ and λ_1 are fitted to match the experiment. It is important to mention, that in case of different apertures of the top and the bottom CC-VCSEL cavities, the two active region temperatures T_i will have different dependence on the injection currents I_i.

A. Steady-state solutions of CC-VCSEL rate equations

In order to find "One-Mode Lasing" regime for the short and the long wavelength fundamental modes, we solve Eq. 1 and Eq. 2 for $N_{ph}^S = N_{ph}^L = 0$ and for both top ($i = 1$) and bottom ($i = 2$) cavities, respectively obtaining [11]:

$$\frac{\eta_1 I_1}{q} - \frac{n_1 V_1}{\tau_e} = 0, \quad (8)$$

$$\frac{\eta_2 I_2}{q} - \frac{n_2 V_2}{\tau_e} = 0, \quad (9)$$

$$\Gamma_{QW,1}^S \, v_g^S \, n_{QW,1} \, g_1^S + \Gamma_{QW,2}^S \, v_g^S \, n_{QW,2} \, g_2^S - \frac{1}{\tau_{ph}^S} = 0, \quad (10)$$

$$\Gamma_{QW,1}^L \, v_g^L \, n_{QW,1} \, g_1^L + \Gamma_{QW,2}^L \, v_g^L \, n_{QW,2} \, g_2^L - \frac{1}{\tau_{ph}^L} = 0. \quad (11)$$

Here $n_{QW,1,2}$ denote the number of QWs in the top and the bottom cavity, respectively.

IV. Simulation of threshold condition

We have performed a numerical simulation based on the rate equations analysis in order to investigate the influence of the CC-VCSELs current apertures on the single and dual wavelength threshold currents.

A. Gain parameters

The gain parameters described by Eqs. 4 - 6 are partially taken from [11], [25] and partially adjusted during optimization and fitting process to the experimental results. The model of temperature dependent gain presented in [25] assumes that the resonant wavelength is within $\pm$ 10 nm away from gain peak λ_p. Although in our simulations temperature range of CC-VCSEL operation shifts the gain peak λ_p a little bit outside of the assumed "window" (e. g. $\lambda_p = 846.2$ nm @ 320 K and $\lambda_p = 861.2$ nm @ 380 K), the results obtained with this model are in a very good agreement with the experiments even for high injection currents. In Tab. I we list all gain parameters used in the simulations.

TABLE I
GAIN PARAMETERS USED IN SIMULATIONS.

a_0	2880	cm^{-1}	
a_1	-1.66	$\mathrm{cm}^{-1}\ \mathrm{K}^{-1}$	
a_2	-0.8 $\times$ 10^{-3}	$\mathrm{cm}^{-1}\ \mathrm{K}^{-2}$	
n_0	1.1 $\times$ 10^{18}	cm^{-3}	
b_0	6.4 $\times$ 10^{9}	cm^{-3}	
b_1	7.67 $\times$ 10^{15}	$\mathrm{cm}^{-3}\ \mathrm{K}^{-1}$	
H_0	1.5 $\times$ 10^{6}	$\mathrm{cm}^{-1}\ \mu\mathrm{m}^{-2}$	$(\lambda > \lambda_p)$
H_0	3.55 $\times$ 10^{6}	$\mathrm{cm}^{-1}\ \mu\mathrm{m}^{-2}$	$(\lambda > \lambda_p)$
λ_0	766	nm	
λ_1	2.501$\times$ 10^{-4}	$\mu\mathrm{m}\ \mathrm{K}^{-1}$	

B. Temperature fit

The experimentally measured wavelength shift with the top and the bottom cavity injection currents can be approximated as:

$$\lambda = \lambda_{T_s} + k(T_a + T_s) \quad (12)$$

with

$$T_a = dI_{TOP} + fI_{BOT}. \quad (13)$$

Here T_s is the surrounding/ambient temperature, k equals to $k = d\lambda/dT$ and parameter d (f) describes the influence of the top (bottom) cavity injection current on the laser active regions temperature rise T_a.
First, we measure the shift of the emitted wavelength with the change of T_s controlled by a Peltier module and determine the k factor:

$$k = \frac{d\lambda}{dT} = \frac{\lambda^{i+1} - \lambda^i}{T_s^{i+1} - T_s^i}. \quad (14)$$

Second, knowing the exact values of the emitted wavelength and the top and the bottom cavity injection currents along the modal threshold curves, we solve the set of Eqs. 12 and extract the d and f parameters:

$$\lambda^i = p_0 + p_1 I_{TOP}^i = p_2 I_{BOT}^i \quad (15)$$

where $p_0 = \lambda_{T_s} + kT_s$, $p_1 = kd$ and $p_2 = kf$.

As an example, we compare in Fig. 7 the experimentally measured wavelength at threshold for type B laser (c.f. Fig. 4) with the theoretical results from the procedure described above. As can be seen, the assumed linear change of the laser temperature with injection currents provides a very good agreement with the experiment. For this case the d, f

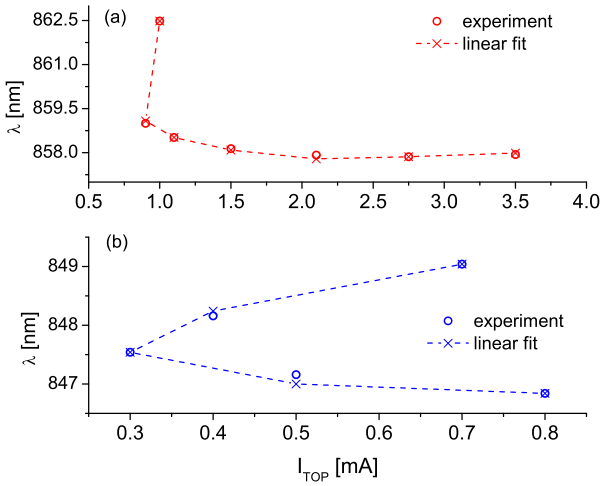

Fig. 7. Experimentally measured wavelength at threshold (open circles) and theoretical results according to Eqns. 12 - 15 for type B laser (crosses).

TABLE II
CC-VCSEL DESIGN.

	no. of layers	layer th. [nm]	x in $Al_xGa_{1-x}As$	dop. lev. [10e+18]	dop. type
Bottom DBR					
n_H	35	60.38	0.16	0.97	p
n_L		67.50	0.92	0.97	p
AlO_x	1	60.38	0.16	0.97	p
	1	68.10	0.98	0.97	p
Cavity Bottom					
spacer	1	79.92	0.20	1E-4	i
QW	5	8.00	0.00	1E-4	i
barrier	4	10.00	0.20	1E-4	i
spacer	1	79.92	0.20	1E-4	i
Middle DBR					
AlO_x	1	68.10	0.98	0.97	n
	1	60.38	0.16	0.97	n
n_L	5	67.50	0.92	0.97	n
n_H		60.38	0.16	0.97	n
Contact layer	1	67.50	0.98	20.00	n++
	1	60.38	0.16	20.00	n++
n_L	5	67.50	0.92	0.97	n
n_H		60.38	0.16	0.97	n
n_L	1	67.50	0.92	0.97	n
Cavity Top					
spacer	1	79.92	0.20	1E-4	i
QW	5	8.00	0.00	1E-4	i
barrier	4	10.00	0.20	1E-4	i
spacer	1	79.92	0.20	1E-4	i
TOP DBR					
n_L	22	67.50	0.92	0.97	p
n_H		60.38	0.16	0.97	p
Contact layer	1	67.50	0.16	20.00	p++
	1	60.38	0.98	20.00	p++

parameters for the short and long wavelength modes are equal to $d_S = 7.93$ K/mA, $f_S = 9.61$ K/mA and $d_L = 9.45$ K/mA, $f_L = 10.18$ K/mA. As the redshift of the emitted wavelength with T_s is induced by the cavity refractive index change, we estimate the thermo-optic coefficient to be equal to $dn/dT = 2.85 \times 10^{-4}$ K^{-1}.

C. CC-VCSEL optical design

D. Simulation results

In Tab. II we present the layer composition of the CC-VCSEL structure.

1) Temperature distribution and B type structure results: First, we resent the results for a typical CC-VCSEL from type B group. Its current apertures are identical to the ones of the CC-VCSEL presented in Fig. 4, i. e. 6 x 6 and 3 x 3 μm^2 for the top and the bottom cavity, respectively. This CC-VCSEL however, is placed in a different wafer unit and therefore, its modal behavior is slightly different (compare Fig. 4 and Fig. 9b). Fig. 8 presents the calculated z-distribution (along the

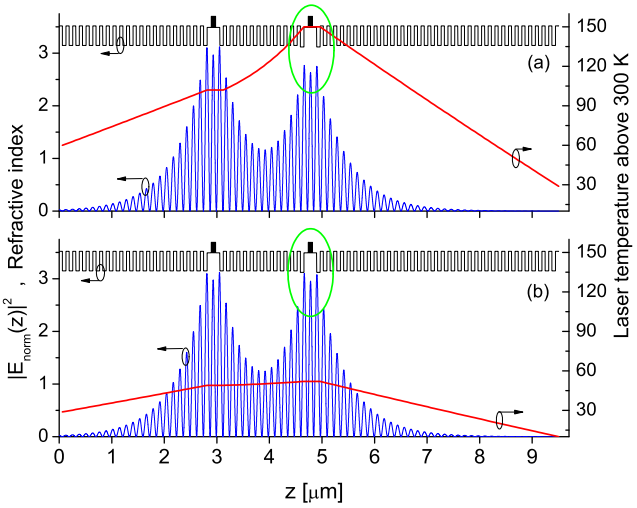

Fig. 8. Optical field distribution of the short wavelength mode, refractive index change and temperature distribution of typical group B CC-VCSEL for top(bottom) injection current: a) $I_{TOP} = 0.6(I_{BOT} = 8)$ mA and b) $I_{TOP} = 4.3(I_{BOT} = 0.5)$ mA.

CC-VCSEL) of the refractive index, temperature and optical power of the short wavelength mode for two sets of injection currents: top (bottom) injection current of a) $I_{TOP} = 0.6$ ($I_{BOT} = 8$) mA and b) $I_{TOP} = 4.3$ ($I_{BOT} = 0.5$) mA. The optical power distribution of the long wavelength mode is quite similar and is not shown.

The temperature distribution is obtained from 2D (r, z) simulations based on the finite element method and, as Fig. 8 shows, it strongly depends on the injection currents and cannot be approximated by an uniform average value. Moreover, it strongly depends on the radii of the two apertures. We find out that a good agreement is achieved when the d and f values are taken separately for the two cavities. The smaller the current aperture, the bigger the temperature coefficients values. This results in a difference of the d^λ and f^λ coefficients extracted from the experiment for the short and the long wavelength mode as the mode confinements in the two cavities are different. The temperature distribution in the DBR regions are approximated by linear functions with boundary condition of 60% of top cavity active region temperature value at the laser facet and 20% of bottom cavity active region temperature value at the substrate interface. Due to the nonuniform temperature distribution along the CC-VCSEL vertical axis, the detinung between the two cavities cased by the thermooptic

effect strongly depends on the injection currents. This can be observed by comparing Fig. 8 a) and b) - quite significant difference in the optical power distribution is visible in the bottom cavity (the region is circled). Table III shows the extracted values of the calculated optical parameters for the two sets of injection currents in Fig. 8 and for no injection currents (300 K uniform).

Heating up of the bottom cavity effectively increases the bottom optical resonator length, and the long wavelength mode jumps from the top cavity (@ 300 K uniform $\Gamma^L_{TOP} > \Gamma^L_{BOT}$) to the bottom cavity ($\Gamma^L_{TOP} < \Gamma^L_{BOT}$). If the CC-VCSEL resonators are not significantly or not at all detuned, the temperature rise caused by the current injection might change the longitudinal modes distribution leading to switching in the emission spectra.

In order to find the active region temperature dependencies on the injection currents for a specific laser, we compare the experimentally measured resonant wavelengths (shown in Figs. 9 a) - 12 b) by open squares and triangles for the short and the long wavelength mode, respectively) with the calculated ones (shown by solid and dashed lines). Knowing the temperature induced refractive index change dn/dT and the designed current apertures, we optimize for each presented laser the d_i and f_i parameters in order to match the experiment. The last step is to adjust the gain parameters (see Tab. I) to match the experimental modal threshold map (see Fig. 9 b)). In such a way, we obtain a very good agreement with the experimental threshold current maps and threshold wavelengths - see Fig. 9. We would like to mention that, as we used 1D transfer matrix method [15] for the optical simulations, we do not account for the resonant wavelength blue-shift due to the transverse optical confinement. Therefore, we use a slight cavity detuning for the different laser groups to compensate these effect.

The only difference between the optimized designs for lasers from each group are the small changes in the top and the bottom cavity spacer thicknesses and the d_i and f_i values. In Tab. IV we list these parameters for type B laser depicted in Fig. 9.

2) C, C+ and A type structures: In Figs. 10, 11 and 12 we compare the experimental and theoretical results for CC-VCSELs from group C, C^+ and A, respectively. The laser parameters are listed in Tables V, VI and VII, respectively. These parameters and the current aperture sizes are the only differences implemented in the simulations that allow to calculate the modal threshold maps for the four different laser groups (see also IV for laser B type) in a very good agreement with experiment. Comparing the experimental data with our simulation results, we notice that the larger the CC-VCSEL current aperture, the more accurate is our theoretical fitting. It is almost ideal in case of lasers with the largest aperture (groups C and C^+) however, for the smallest apertures the thermal impact becomes very significant and our modeling becomes less accurate.

TABLE III
B - TYPE STRUCTURE FOR DIFFERENT CURRENT INJECTION LEVELS (SEE DESCRIPTION OF 8).

T	300 K uniform	point (a)	point (b)	
Γ^S_{top}	1.78	1.90	2.00	%
Γ^S_{bot}	2.03	1.88	1.77	%
Γ^L_{top}	1.97	1.83	1.68	%
Γ^L_{bot}	1.76	1.87	1.92	%
G^S_{th}	763	784	802	cm^{-1}
G^L_{th}	834	844	907	cm^{-1}
λ^S	845.22	847.82	852.31	nm
λ^L	855.72	858.41	863.11	nm

TABLE IV
B - TYPE STRUCTURE OPTIMIZED PARAMETERS.

Cav_{TOP} spacers	81.26	nm
Cav_{BOT} spacers	80.26	nm
Cav_{TOP} aperture	6 x 6	μm^2
Cav_{BOT} aperture	3 x 3	μm^2
d_{TOP}	10	K/mA
f_{TOP}	12	K/mA
d_{BOT}	10	K/mA
f_{BOT}	18	K/mA

TABLE V
C - TYPE STRUCTURE OPTIMIZED PARAMETERS.

Cav_{TOP} spacers	81.86	nm
Cav_{BOT} spacers	80.56	nm
Cav_{TOP} aperture	6 x 6	μm^2
Cav_{BOT} aperture	5 x 5	μm^2
d_{TOP}	10	K/mA
f_{TOP}	4	K/mA
d_{BOT}	4	K/mA
f_{BOT}	5	K/mA

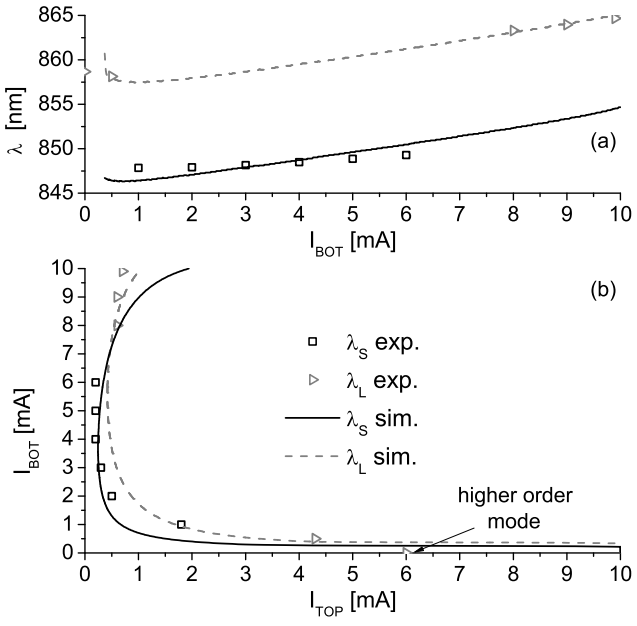

Fig. 9. Wavelengths at laser threshold (a) and modal threshold map (b). Experimental results are shown by open squares and triangles for the short and the long wavelength mode, respectively while the calculated ones - by solid and dashed line. CC-VCSEL from group B with 6 x 6 and 3 x 3 μm^2 top and bottom cavity current apertures.

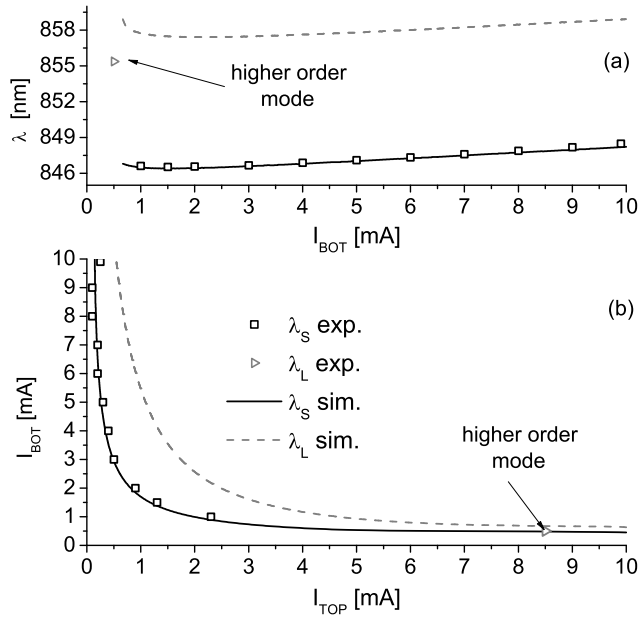

Fig. 10. Same as 9 but for CC-VCSEL from group C with 6 x 6 and 5 x 5 μm^2 top and bottom cavity current apertures.

TABLE VI
C$^+$ - TYPE STRUCTURE OPTIMIZED PARAMETERS.

Cav$_{TOP}$ spacers	82.56	nm
Cav$_{BOT}$ spacers	81.26	nm
Cav$_{TOP}$ aperture	6 x 6	μm^2
Cav$_{BOT}$ aperture	9 x 9	μm^2
d_{TOP}	10	K/mA
f_{TOP}	5	K/mA
d_{BOT}	3	K/mA
f_{BOT}	2.5	K/mA

TABLE VII
A - TYPE STRUCTURE OPTIMIZED PARAMETERS.

Cav$_{TOP}$ spacers	77.06	nm
Cav$_{BOT}$ spacers	77.06	nm
Cav$_{TOP}$ aperture	5 x 5	μm^2
Cav$_{BOT}$ aperture	2.2 x 2.2	μm^2
d_{TOP}	10	K/mA
f_{TOP}	15	K/mA
d_{BOT}	10	K/mA
f_{BOT}	23	K/mA

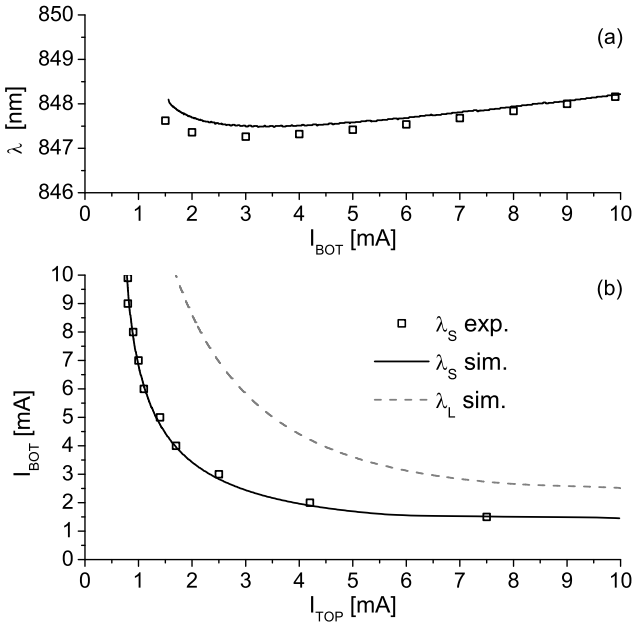

Fig. 11. Same as 9 but for CC-VCSEL from group C$^+$ with 6 x 6 and 9 x 9 μm^2 top and bottom cavity current apertures.

E. Conclusions

We carry out a detailed characterization of CW threshold behaviour of a number of Coupled-Cavity VCSELs with various radii of the ion-implantation and oxide apertures. We obtain modal threshold current maps and wavelength at threshold. We identify four groups of lasers with qualitatively different behavior, i. e. lasing only on the short, on the long or on both short and long wavelength fundamental modes. All those groups show a profound impact of the active and/or passive regions current induced self-heating. In order to elucidate this impact, we improve the existing rate equation model by adding gain and refractive index temperature dependencies. We are able to reproduce the experimentally observed switching between the long and the short wavelength fundamental modes. For all presented cases, the tendencies measured in the experiment are repeated in simulations and we are able to simulate the four different typical modal behaviors.

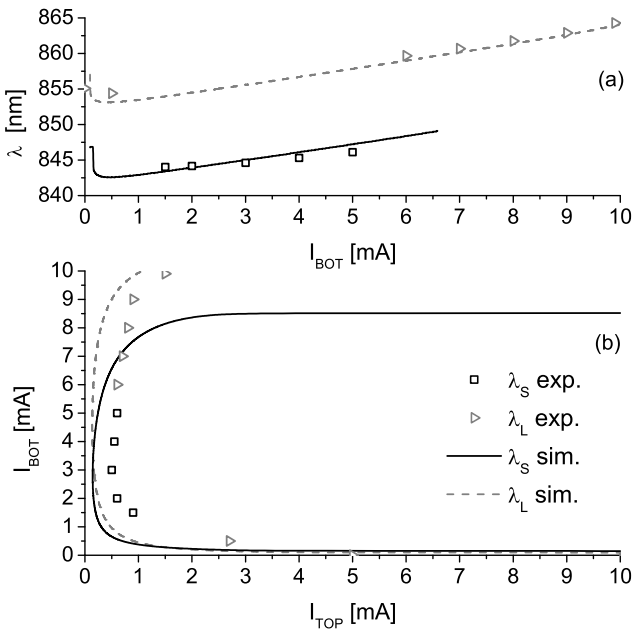

Fig. 12. Same as 9 but for CC-VCSEL from group A with 5 x 5 and 2.2 x 2.2 μm^2 top and bottom cavity current apertures.

REFERENCES

[1] S. F. Yu, "Analysis and design of vertical cavity surface emitting lasers," *Analysis and Design of Vertical Cavity Surface Emitting Lasers, by SF Yu, pp. 464. ISBN 0-471-39124-7. Wiley-VCH, August 2003.*, vol. 1, 2003.

[2] T. Numai, *Fundamentals of semiconductor lasers*. Springer, 2004, vol. 93.

[3] T. E. Sale, *Vertical cavity surface emitting lasers*. Research Studies Press Taunton, Somerset, 1995.
[4] L. A. Coldren, S. W. Corzine, and M. L. Mashanovitch, *Diode lasers and photonic integrated circuits*. Wiley, 2012.
[5] R. Stanley, R. Houdre, U. Oesterle, M. Ilegems, and C. Weisbuch, "Coupled semiconductor microcavities," *Appl. Phys. Lett.*, vol. 65, no. 16, pp. 2093–2095, 1994.
[6] P. Pellandini, R. Stanley, R. Houdre, U. Oesterle, M. Ilegems, and C. Weisbuch, "Dual-wavelength laser emission from a coupled semiconductor microcavity," *Appl. Phys. Lett.*, vol. 71, no. 7, pp. 864–866, 1997.
[7] P. Michler, M. Hilpert, and G. Reiner, "Dynamics of dual-wavelength emission from a coupled semiconductor microcavity laser," *Appl. Phys. Lett.*, vol. 70, no. 16, pp. 2073–2075, 1997.
[8] J. Carlin, R. Stanley, P. Pellandini, U. Oesterle, and M. Ilegems, "The dual wavelength bi-vertical cavity surface-emitting laser," *Appl. Phys. Lett.*, vol. 75, no. 7, pp. 908–910, 1999.
[9] A. Fischer, K. Choquette, W. Chow, H. Hou, and K. Geib, "Coupled resonator vertical-cavity laser diode," *Appl. Phys. Lett.*, vol. 75, no. 19, pp. 3020–3022, 1999.
[10] M. Brunner, K. Gulden, R. Hovel, M. Moser, J. Carlin, R. Stanley, and M. Ilegems, "Continuous-wave dual-wavelength lasing in a two-section vertical-cavity laser," *IEEE Phot. Technol. Lett.*, vol. 12, no. 10, pp. 1316–1318, 2000.
[11] V. Badilita, J.-F. Carlin, M. Ilegems, and K. Panajotov, "Rate-equation model for coupled-cavity surface-emitting lasers," *IEEE J. Quantum Electron.*, vol. 40, no. 12, pp. 1646–1656, 2004.
[12] V. Badilita, J.-F. Carlin, M. Brunner, and M. Ilegems, "Light-current characterization of dual-wavelength vcsels," in *Symposium on Integrated Optoelectronic Devices*. International Society for Optics and Photonics, 2002, pp. 87–95.
[13] V. Badilita, J.-F. Carlin, M. Ilegems, M. Brunner, G. Verschaffelt, and K. Panajotov, "Control of polarization switching in vertical coupled-cavities surface emitting lasers," *IEEE Phot. Technol. Lett.*, vol. 16, no. 2, pp. 365–367, 2004.
[14] D. M. Grasso and K. D. Choquette, "Temperature-dependent polarization characteristics of composite-resonator vertical-cavity lasers," *IEEE J. Quantum Electron.*, vol. 41, no. 2, pp. 127–131, 2005.
[15] K. P. Panajotov, M. Zujewski, and H. Thienpont, "Coupled-cavity surface-emitting lasers: spectral and polarization threshold characteristics and electrooptic switching," *Optics Express*, vol. 18, no. 26, pp. 27 525–27 533, 2010.
[16] J. A. Hudgings, R. J. Stone, C.-H. Chang, S. F. Lim, K. Y. Lau, and C. J. Chang-Hasnain, "Dynamic behavior and applications of a three-contact vertical-cavity surface-emitting laser," *IEEE J. Select. Topics Quantum Electron.*, vol. 5, no. 3, pp. 512–519, 1999.
[17] J. A. Hudgings, R. J. Stone, S. F. Lim, G. S. Li, W. Yuen, K. Y. Lau, and C. J. Chang-Hasnain, "The physics of negative differential resistance of an intracavity voltage-controlled absorber in a vertical-cavity surface-emitting laser," *Appl. Phys. Lett.*, vol. 73, no. 13, pp. 1796–1798, 1998.
[18] J. A. Hudgings, R. J. Stone, S. F. Lim, K. Y. Lau, and C. J. Chang-Hasnain, "Comparative study of the analog performance of a vertical-cavity surface-emitting laser under gain and cavity loss modulation," *Appl. Phys. Lett.*, vol. 77, no. 14, pp. 2092–2094, 2000.
[19] A. J. Fischer, K. D. Choquette, W. W. Chow, A. A. Allerman, and K. M. Geib, "Bistable output from a coupled-resonator vertical-cavity laser diode," *Appl. Phys. Lett.*, vol. 77, no. 21, pp. 3319–3321, 2000.
[20] A. J. Fischer, W. W. Chow, K. D. Choquette, A. A. Allerman, and K. M. Geib, "Q-switched operation of a coupled-resonator vertical-cavity laser diode," *Appl. Phys. Lett.*, vol. 76, no. 15, pp. 1975–1977, 2000.
[21] D. M. Grasso and K. D. Choquette, "Threshold and modal characteristics of composite-resonator vertical-cavity lasers," *IEEE J. Quantum Electron.*, vol. 39, no. 12, pp. 1526–1530, 2003.
[22] A. Fischer, K. Choquette, W. Chow, A. Allerman, D. Serkland, and K. Geib, "High single-mode power observed from a coupled-resonator vertical-cavity laser diode," *Appl. Phys. Lett.*, vol. 79, no. 25, pp. 4079–4081, 2001.
[23] V. Badilita, J.-F. Carlin, M. Brunner, and M. Ilegems, "Light-current characterization of dual-wavelength vcsels," in *Symposium on Integrated Optoelectronic Devices*. International Society for Optics and Photonics, 2002, pp. 87–95.
[24] A. C. Lehman and K. D. Choquette, "Threshold gain temperature dependence of composite resonator vertical-cavity lasers," *IEEE J. Select. Topics Quantum Electron.*, vol. 11, no. 5, pp. 962–967, 2005.
[25] J. S. Gustavsson, J. A. Vukusic, J. Bengtsson, and A. Larsson, "A comprehensive model for the modal dynamics of vertical-cavity surface-emitting lasers," *IEEE J. Quantum Electron.*, vol. 38, no. 2, pp. 203–212, 2002.

Mateusz Zujewski was born in Poland in 1984. He received his MSc degree in Computer Physics from the Faculty of Technical Physics, Computer Science and Applied Mathematics of the Technical University of Lodz, Poland. Since 2009 he is working toward his PhD degree at B-PHOT - Department of Applied Physics and Photonics, Vrije Universiteit Brussel, Brussels.